JOURNAL OF CATALYSIS 35, 256–272 (1974)

Composition and Catalytic Properties of Synthetic Ferrierite

C. L. KIBBY, A. J. PERROTTA* AND F. E. MASSOTH

Gulf Research & Development Company, Pittsburgh, Pennsylvania 15230

Received May 9, 1974

Synthetic sodium and sodium-tetramethylammonium ferrierites were prepared under hydrothermal conditions at 300–325°C. With seeding, the syntheses were completed in 2 hr. The alkali forms could be converted to hydrogen ferrierite by direct exchange with mineral acids, as well as by the usual ammonium ion exchange and calcination.

Hydrogen ferrierite is an active and very selective catalyst for *n*-paraffin cracking. It has effective pore openings of about 5 Å, and sorption capacities of 0.05–0.09 cc/g for light *n*-paraffins, but only 0.002–0.01 cc/g for isoparaffins and aromatics. It is stable to 950°C in air, but loses cracking activity if steamed at 750°C.

INTRODUCTION

Ferrierite is a magnesium zeolite first discovered by Graham near Kamloops Lake, British Columbia (*1*). Powder X-ray data for that mineral were reported by Staples (*2*) and crystal structures were determined by Vaughn (*3*) and Kerr (*4*). Its unit cell is orthorhombic with dimensions $a = 19.16$ Å, $b = 14.13$ Å, $c = 7.49$ Å, and composition approximately $Na_2Mg_2Al_6Si_{30}O_{72} \cdot 18\ H_2O$ (*3*). Other occurrences of ferrierite have been reported in Bulgaria (*5*), Italy, (*6*), Yugoslavia, (*7*), Japan (*8*), and in the western U. S. (*9*, *10*). It is found in cavities in volcanic rocks and is associated with quartz (chalcedony) or calcite (*9*). Substitutions of Ca^{2+}, Fe^{2+}, and K^+ for Na^+ Mg^{2+} in exchange cation positions, and of the Fe^{3+} for Al^{3+} and Si^{4+} in lattice positions, are all found in mineral ferrierites, and the Si/Al ratio varies from four to seven (*1*, *5–10*).

A representation of the ferrierite structure is shown in Fig. 1. The structure contains dense layers of interlinked five-membered rings of $(Al,Si)O_4$ tetrahedra, perpendicular to the *a*-axis, which are separated by 6-, 8-, and 10-membered ring channels. The 8-ring channels run in the 010 (*b*-axis) direction and intersect both 6- and 10-ring channels which run in the 001 (*c*-axis) direction. Cavities of 6 to 7 Å diameter are formed by the intersections of six- and eight-ring channels; there are two of these per unit cell which contain the magnesium ions in mineral ferrierites (*3*). The free diameter of the main 10-ring channels (two per unit cell) is slightly over 5 Å (*3*, *4*).

Ferrierite was first synthesized unknowingly by Coombs *et al.* (*11*) from mixed sodium–calcium compositions heated hydrothermally to 330°C. With sodium or calcium alone, they found only mordenite and analcite. However, Senderov (*12*) reported a calcium-free ferrierite from H_2O-rich mordenite preparations containing excess Na_2O; and a similar study by Sands (*13*) also revealed the coexistence of sodium ferrierite with mordenite, quartz, and analcite. Barrer and Marshall (*14*) synthesized a strontium zeolite which they later identified as ferrierite (*15*), and Hawkins (*16*) reported both calcium and strontium ferrierites from oxide mixtures with compositions $CaO(SrO):Al_2O_3:7SiO_2$.

We report the synthesis of sodium and sodium-tetramethylammonium ferrierites,

* To whom all inquiries should be addressed.

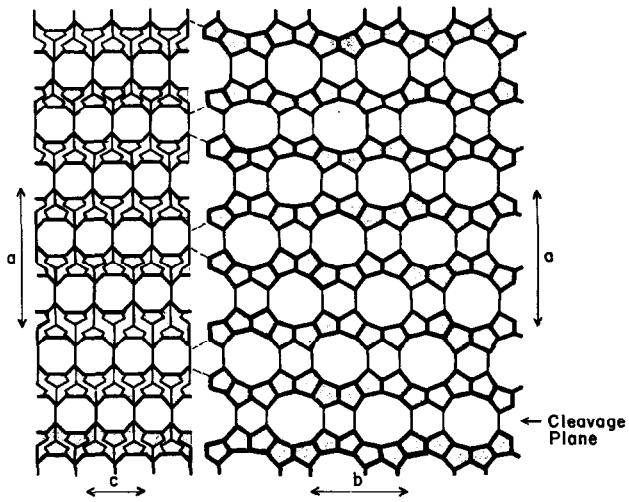

FIG. 1. Ferrierite structure [as in Ref. (4)].

and physical and chemical properties of these and of sorbents and catalysts derived from them.

EXPERIMENTAL METHODS

A. Synthesis

The starting materials for ferrierite synthesis were reagent grade sodium aluminate (Fisher) and Ludox AS (DuPont), a colloidal form of silica stabilized by ammonia (0.25% NH_3; 30.1 wt% SiO_2; pH 9.6). In a typical batch synthesis, 21.8 g of sodium aluminate, $Na_2O:Al_2O_3:3H_2O$, was dissolved in 200 cc H_2O, then 200 g Ludox AS added with vigorous stirring to form a gel. The gel was transferred to a 3.3 cm i.d. × 75 cm long Pyrex tube equipped with a thermocouple well. The tube was inserted into a hydrothermal bomb, the remainder of the gel washed into it with another 100 cc H_2O, and 50 cc H_2O added to the bottom of the reactor before it was closed. The temperature was brought up to 300–325°C in about 2 hr, then held there for 72 hr (soak time). The temperature was measured by iron–iron constantan thermocouples; it was controlled to ±3°C. Reactor pressure was established by the water vapor pressure at reactor temperature (1250–1800 psi). After cooling to room temperature (about 2 hr), the ferrierite crystals were washed free from the bottom of the Pyrex tube and washed thoroughly with water to remove any entrapped sodium silicate. In some runs, 50 g of tetramethylammonium hydroxide solution (Eastman Kodak, 10% in H_2O) were added to the sodium aluminate before addition of the Ludox AS. In seeded runs, 1 g of ferrierite crystals was stirred into the gel just before it was transferred to the Pyrex tube.

B. Conversion to Hydrogen Form

Acid leaching of ferrierite crystals was routinely accomplished by stirring the crystals in 2 *N* HCl at 85°C. Ammonium exchange for sodium ions was also done in batches using 2 *N* NH_4NO_3 or NH_4Cl solutions at 85–90°C. In the latter case, the crystals were calcined at 450–550°C between steps and a final calcination given to convert the ammonium form to the hydrogen form. The Na-TMA ferrierite was calcined in air at 500°C prior to ion exchanging.

C. Physical Characterization

X-Ray powder diffraction data were obtained on a Picker diffractometer using Cu-$K\alpha$ radiation. A novaculite specimen was used as an external standard. Electron diffraction data were obtained with a Phillips 300 electron microscope, and photomicrographs were made with a JEOLCO scanning electron microscope. Thermo-

gravimetric data were obtained with a Fisher dual TGA-DTA instrument and with a Cahn electrobalance equipped for flow measurements (*17*). Surface areas were determined by the BET adsorption method using N_2. Chemical analysis was by X-ray fluorescence.

D. Sorption Studies

Sorption measurements were made on a flow microbalance and also by a gas chromatographic technique. On the microbalance, 200 mg samples in a quartz bucket were suspended in a quartz tube heated by a split-shell furnace. Upflow was employed with a bed of quartz beads at the bottom of the reactor for preheating the incoming gases. A thermocouple was positioned immediately below the sample. Gas flows were metered by calibrated rotometers; liquids were introduced by passing an inert gas (He or N_2) through bubbler saturators maintained at room temperature (about 22°C). Sorptions were usually carried out with the samples at 66°C, after an overnight pretreatment in air, He or N_2 at 540°C. Weights were corrected for gas buoyancy effects.

In the chromatographic technique, pulses or continuous flows of the desired sorbates were injected into a 50 cc/min He or N_2 flow and passed over 0.1–1.0 g samples in an eight mm o.d. quartz U-tube reactor. The samples were pretreated overnight in O_2 or He at 540°C, and the sorptions were measured at about 22°C. All of the carrier gases were dried with molecular sieves, and the hydrocarbon sorbates were all of high purity as determined by gc analysis (most were 99+% purity from Chem Samp Co.). The reactor was connected directly to a gas chromatograph so that the sorptions of several compounds could be measured simultaneously. Also, the gases desorbed (as by heating) were analyzed to check for chemical reaction.

E. Catalytic Tests

Cracking activity tests were made with the same quartz microreactor used for sorption measurements. Pulse and continuous flow techniques were used with both He and H_2 as carrier gases.

Results and Discussion

Synthesis

Sodium ferrierite was initially made on a small scale (10 g of product) at 290–325°C. The phase distributions, as deter-

TABLE 1
Small-Scale Synthesis Data for Ferrierite

Run	Composition (moles)	T (°C)	Time (hr)	P (psi)	Phases present (remarks)[a]
APZ 1-13	$Na_2O{\cdot}Al_2O_3{\cdot}10SiO_2$	282–288	119	975–1060	Mordenite, analcite, amorphous pH 9 of end liquor
APZ 1-15	$Na_2O{\cdot}Al_2O_3{\cdot}10SiO_2$	296–305	72	1180–1350	Ferrierite, analcite, mordenite
APZ 1-16	$Na_2O{\cdot}Al_2O_3{\cdot}12SiO_2$	293–299	40	1140–1225	Ferrierite (analcite, mordenite) pH 8.8 of end liquor
APZ 1-17	$Na_2O{\cdot}Al_2O_3{\cdot}8SiO_2$	291–300	55	1100–1250	Ferrierite, mordenite, analcite pH 8 of end liquor
APZ 1-79	$Na_2O{\cdot}Al_2O_3{\cdot}12SiO_2$	298–310	41	1200–1400	Ferrierite, analcite
APZ 1-55	$Na_2O{\cdot}Al_2O_3{\cdot}12SiO_2$	294–299	63	1150–1225	Ferrierite, amorphous
APZ 1-57	$Na_2O{\cdot}Al_2O_3{\cdot}12SiO_2$	296–307	52	1180–1400	Ferrierite, analcite
APZ 1-63	$Na_2O{\cdot}Al_2O_3{\cdot}12SiO_2$	298–326	69	1200–1750	Analcite, ferrierite (mordenite)
APZ 1-73	$Na_2O{\cdot}Al_2O_3{\cdot}12SiO_2$	291–300	52	1100–1425	Ferrierite (analcite, mordenite)
APZ 1-76	$Na_2O{\cdot}Al_2O_3{\cdot}12SiO_2$	290–313	68	1100–1490	Ferrierite, analcite (mordenite)
APZ 1-86	$Na_2O{\cdot}Al_2O_3{\cdot}12SiO_2$	293–304	63	1140–1340	Ferrierite, analcite spheroids with scanning electron microscopy
APZ 1-89	$Na_2O{\cdot}Al_2O_3{\cdot}12SiO_2$	291–305	51	1100–1350	Ferrierite, mordenite (analcite)

[a] Phases in parentheses indicate a minor amount.

mined by X-ray powder data, and the synthesis conditions are shown in Table 1. At lower temperatures, mordenite crystallized as the major phase, in accord with earlier work (*11–13*). Analcite crystallized as the major phase above 325°C.

Scale-up runs (to 70 g) gave low yields of ferrierite crystals at first; the major phase was amorphous. It was believed that nucleation of ferrierite crystals started at the walls of the Pyrex tube containing the gel. When the diameter of the tube was halved to 3.3 cm, giving a surface/volume ratio similar to that in the smaller-scale runs, high yields of ferrierite were formed with very little amorphous material. In most preparations, small amounts of analcite were also formed and at times both mordenite and quartz were detected.

Intensities of the (200) X-ray reflections were used to estimate the degree of crystallinity of preparations. Plots of I (200) versus soaking time at 310°C are shown in Fig. 2. A soaking time of 72 hr was normally used to assure complete crystallization. Fairly large crystals (10–100 μm) were formed which could be examined by reflection microscopy at magnifications of 90–210×. Using crystals of this size to seed new preparations, the soaking time was reduced to as little as 2 hr at 310°C.

Attempts were made to prepare a hydrogen ferrierite directly using tetramethylammonium (TMA) ions in the synthesis. Complete substitution of TMA for sodium was not successful, but mixed TMA-Na ferrierites did crystallize with about one-third of the sodium ions replaced by TMA ions. Generally, the crystallinity was improved when TMA ions were present.

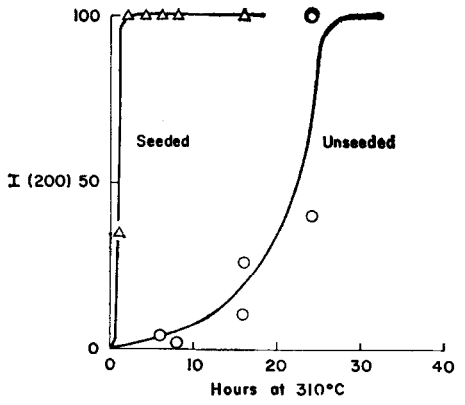

FIG. 2. Kinetics of ferrierite crystallization.

The hydrogen form of ferrierite was made from the sodium form by treatment with strong acid solutions (e.g., 2 N HCl at 90°C). By using a large excess of acid and more than one leaching step, fairly low sodium levels ($\leq$0.4 wt%) were achieved in batch operation. Soxhlet extraction with constant boiling HCl (6 N, 109°C) reduced the sodium content to 0.1 wt% (by X-ray fluorescence analysis). Ammonium ion exchange was not as effective as treatment with acid, especially in opening up the pore system; only a few Na-ferrierites were converted to acid forms by ammonium ion exchange and calcination. However, the TMA-Na ferrierites could readily be converted to hydrogen ferrierite by ammonium ion exchange, after the TMA ions were decomposed by air calcination, and most of the TMA preparations were transformed in this way rather than by acid treatment.

Chemical Analysis

The unit cell of ferrierite has the generalized formula: $(Na,K)_x(Mg,Ca)_yAl_{x+2y}Si_{36-x-2y}O_{72}\cdot 18H_2O$. The minerals also have iron present in the lattice (Fe^{3+}) or exchange cation (Fe^{2+}) positions. In most cases the exchange cation charges balance the aluminum content quite well, although there is sometimes an excess of alkali as in Graham's analysis of the Kamloops Lake ferrierite (*1*, *3*). For both sodium and sodium-TMA ferrierites, the Si/Al ratio varied from 5 to 7 (x = 4.5–6). This is within the range of Si/Al ratios found in mineral ferrierites (4–7).

The hydrogen forms of ferrierite made by acid leaching of the sodium forms have essentially the same Si/Al ratios; even Soxhlet extraction with constant boiling HCl increased the Si/Al ratio by only 10%. Slight loss of material generally occurred during acid treatment, but this was mainly due to physical loss of fines and dissolution of amorphous material or low silica phases such as analcite. As has been

noted by Bogdanova and Belitskii (*18*), ferrierite is very stable in acid solutions.

Diffraction Data—Morphology

Powder X-ray diffraction data for a well-crystallized sample of sodium ferrierite are given in Table 2. The (200) reflection was most intense, while the (110) reflection present in some mineral ferrierites was absent. For comparison, reflections of several natural and synthetic ferrierites are given.

The morphology of sodium ferrierite crystals was observed with a scanning electron microscope. In Fig. 3, they are seen to be comprised of octagonal platelets stacked like a deck of cards. This is not surprising, considering the layered structure shown in Fig. 1. The octagonal faces of the crystals shown are about 10 μm wide, and the stacks are about 10 μm thick. None of the platelets appears to be thicker than about 1 μm; there are 20 or more in each bundle of crystals. Assuming an average thickness of 0.5 μm, the external surface area of the basic platelet is about 2 m^2/g.

Other crystal habits were observed. The spheres in Fig. 3B are either analcite or amorphous material; columnar crystals (Fig. 3A), possibly quartz or albite, were present in minor amounts and were not positively identified. Lath-shaped crystals having a sheaf-like internal structure were identified as mordenite; these could be eliminated from most preparations by keeping the soak temperature above 310°C.

An electron diffraction spot pattern was obtained from a ferrierite platelet with the electron beam normal to the platelet faces.

TABLE 2
X-RAY POWDER DATA FOR FERRIERITES

	Synthetic						Natural					
	Sodium[a]		Strontium[b]		Sr-D[c]		Kamloops[d]		Agoura[e]		Sonora Pass[e]	
hkl	*d* (Å)	I/I_0	*d* (Å)	I/I_0	*d* (Å)	I/I_0	*d* (Å)	I/I_0	*d* (Å)	I/I_0	*d* (Å)	I/I_0
110							11.3	20	11.3	3		
200	9.41 (9.57)	100 (100)	9.45	40	9.49	75	9.61	100	9.47	50	9.56	80
020	7.00 (7.12)	24 (20)	7.02	10	7.07	20	7.00	30	7.07	38	7.06	12
011	6.56 (6.70)	24 (20)	6.58	30	6.61	55	6.61	20	6.59	3	6.61	8
310	5.72 (5.68)	12 (40)	5.77	10	5.77	15	5.84	50	5.75	15	5.83	21
220	5.61	12							5.64	14	5.71	8
031	3.97 (4.00)	45 (80)	3.97	50	3.99	45	3.99	90	3.98	35	3.99	29
420	3.92	37	3.94	40	3.94	35			3.94	35	3.97	60
411	3.83	27	3.86	40	3.86	25	3.88	10				
330	3.75 (3.76)	40 (60)	3.78	50	3.78	50	3.79	20	3.78	65	3.79	55
510	3.65 (3.66)	34 (40)	3.66	30	3.67	30	3.69	50	3.66	12	3.70	37
040	3.52 (3.57)	65 (50)	3.52	100	3.54	90	3.54	80	3.54	100	3.53	100
202	3.47 (3.49)	58 (70)	3.47	80	3.48	100	3.49	80	3.48	18	3.49	50
240	3.30 (3.33)	15 (10)	3.31	20	3.31	20	3.31	20	3.31	35	3.32	13
312	3.15 (3.15)	28 (40)	3.14	50	3.14	55	3.15	30	3.14	12	3.15	9
431	3.04 (3.06)	20 (20)	3.05	40	3.06	45	3.07	30	3.05	12	3.07	13
530	2.94	10	2.95	30	2.96	25	2.97	30			2.98	22
620	2.88 (2.91)	10 (10)	2.89	40	2.90	35	2.90	20				
350	2.56 (2.57)	3 (10)	2.60	10	2.58	10	2.58	30	2.58	10		

[a] Initial entries from this work. Values in parentheses from Ref. (*12*).
[b] From Ref. (*16*)
[c] From Ref. (*15*).
[d] From Ref. (*2*).
[e] From Ref. (*9*).

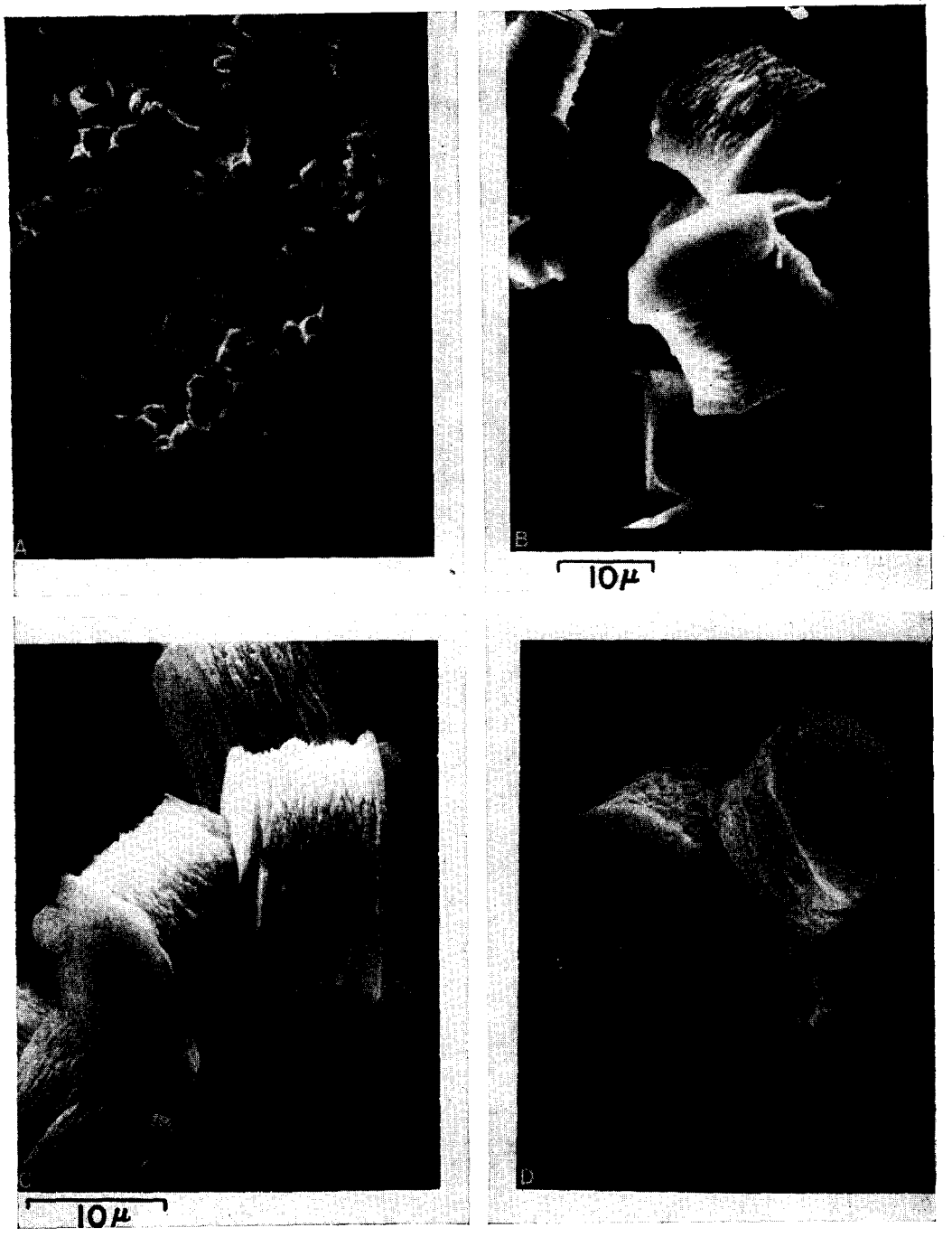

FIG. 3. Electron micrographs of ferrierite. (A) 280×, ferrierite crystals plus some unidentified columnar crystals and spheres; (B) 1400×; (C) 2100×, side view showing stacking of crystallites; (D) 2100×, top view showing octagonal platelets of ferrierite.

Repeat distances of $b = 14.0$ Å and $c = 7.4$ Å were obtained; thus, the platelet faces are parallel to (100) planes. The main 10-ring channels and the 8-ring channels (Fig. 1) run parallel to the platelet faces and have openings at their edges.

Thermogravimetric Analyses

Weight losses on heating are shown in Fig. 4 for sodium, sodium-TMA, and hydrogen forms of ferrierite. A sodium form lost 8.4% of its weight when heated to 950°C, while the hydrogen form derived from it lost 12.2%. The structures were still intact at that temperature. Heating to 1200°C completely degraded the structures (forming a glass which contained a few cristobalite crystals) and caused an additional 1% weight loss. From the weight losses and X-ray fluorescence analyses for Na, Al, and Si, the average compositions were $Na_5Al_5Si_{31}O_{72}\cdot 13H_2O$ for sodium ferrierite and $H_{4.5}Na_{0.5}Al_5Si_{31}O_{72}\cdot 18H_2O$ for hydrogen ferrierites. A dehydrated hydrogen ferrierite only regained 8.3% of its original weight when it was cooled to 20°C and contacted with a flow of air saturated with water.

A fresh Na-TMA ferrierite lost 9.7% of its weight when heated in air to 950°C. Part of the extra weight loss was due to decomposition of TMA ions, which replaced about one-third of the sodium ions. Although comparable sodium levels were reached, hydrogen ferrierites derived from the Na-TMA forms by ammonium ion exchange gave lower weight losses than acid-leached samples (Fig. 4). The difference was about $2H_2O$ per unit cell.

Thus, only for acid-extracted hydrogen ferrierites did the water contents reach $18H_2O$ per unit cell as reported for mineral ferrierites (*1*, *9*). Some of the water must be replaced by sodium ions in the alkali forms. For all of the samples, only 12 or $13H_2O$ molecules per unit cell were easily desorbed and/or readsorbed. This corresponds to a volume of 0.080–0.090 ml/g.

Sorption Properties

With a diameter of about 5 Å, the main channels of ferrierite should admit small molecules such as *n*-paraffins, but exclude large molecules such as isoparaffins and six-membered ring aromatics. Barrer and Lee (*19*) did find that a hydrogen ferrierite, made by treatment of strontium ferrierite with HCl, sorbed 60–80 mg/g of pyrrole

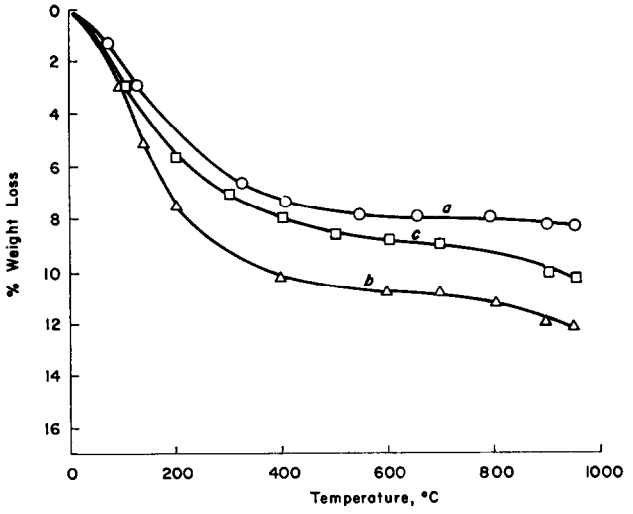

FIG. 4. Thermogravimetric analyses of ferrierite (10°C/min in air). (a) Sodium ferrierite; (b) HCl-treated form of (a), with 0.5% Na_2O; (c) calcined, ammonium ion exchanged form of sodium-TMA ferrierite, with 0.5% Na_2O.

and thiophene, but only 10–20 mg/g of benzene or xylenes.

The capacity of the main channels should be about 60–85 μl/g, assuming an average cross section of 18–23 Å^2. In the synthetic sodium form, the channels were blocked not only to hydrocarbons but to molecules as small as nitrogen. For example, a typical sodium ferrierite sorbed only 0.9 μl/g of *n*-octane and had a BET surface area of 7 m^2/g (7 m^2/g = 2.5 μl/g, assuming a N_2 monolayer thickness of 3.54 Å). The channels could be partially opened by ammonium ion exchange, so that the BET areas increased to 100 m^2/g, but appreciable capacities for *n*-paraffins were not created unless a more severe treatment was used. Stirring in hot HCl or other strong mineral or organic acids was effective in increasing BET areas to 150–200 m^2/g and *n*-paraffin sorption capacities to 50–90 μl/g. In Fig. 5, nitrogen and *n*-octane sorption capacities are shown for a sodium ferrierite sample after extraction by constant boiling HCl. Also shown is the variation in the residual sodium content. Only a brief exposure to this rather severe treatment was sufficient to exchange 80% of the sodium and to develop 80% of the maximum sorption capacity for nitrogen. The volume available to nitrogen closely followed the

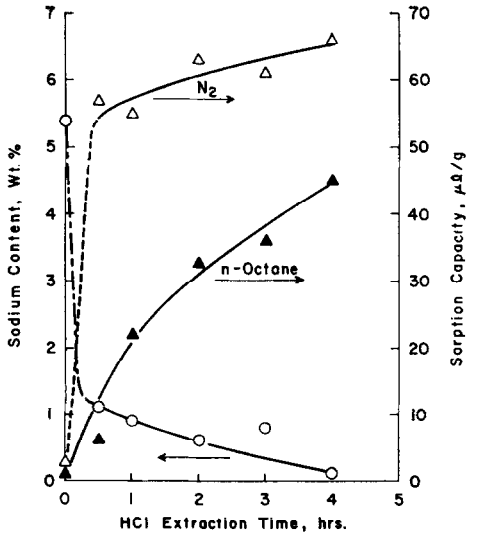

FIG. 5. Sorption capacity of ferrierite developed by HCl extraction.

sodium content, but the *n*-octane capacity increased more slowly and was fully developed only after almost all of the sodium was exchanged. This is the behavior expected if *n*-octane enters only the main channels and sodium ions block them, since all of the volume between any two remaining ions would be inaccessible even though all of the sodium ions in it were removed. Molecules as small as nitrogen may pass through the eight-membered ring channels and thereby by-pass obstructing sodium ions in the main channels.

However, when an acid-extracted ferricrite, with 0.5% Na_2O and a sorption capacity of 63 μl/g for *n*-heptane, was back-exchanged with sodium ions, to 3.0% Na_2O, its *n*-heptane sorption capacity was still 40 μl/g. Evidently the pore system was initially blocked by more than just sodium ions; acid treatment removed extra "amorphous material" as well as exchanging H_3O^+ for Na^+.

Preparations using TMA ions also had BET areas of 7–8 m^2/g after oven drying, but calcination in air at 400–500°C increased the areas to about 100 m^2/g, and *n*-octane sorption capacities of 30–40 μl/g were created by ammonium ion exchange after calcination.

In Fig. 6, the rate of sorption of *n*-heptane at 66°C is shown for a well-crystallized ferrierite, after acid treatment which reduced the sodium content to below 0.5 wt%. An initial rapid weight gain was followed by a slower, continuous increase. After several hours the weight change was small but still continuing; about 10% additional weight was gained overnight. Sorption capacities were arbitrarily chosen as those for 4-hr exposures at a partial pressure 0.8 times the vapor pressure of heptane at 20°C. Sorption of *n*-heptane was only partially reversible at 66°C. About 10–15% was desorbed in 1 hr in N_2 or He; continued desorption was very slow. Upon heating, rapid desorption commenced at 150°C, but complete removal was not achieved even at 550°C as some of the hydrocarbon was converted to "coke." The residue could be removed only by burning in air above 400°C.

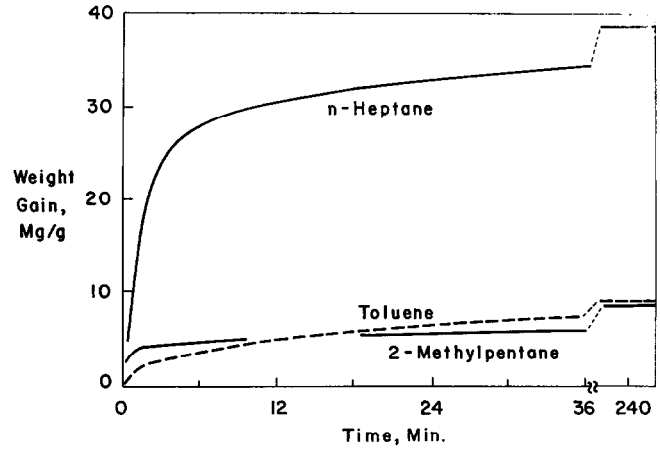

FIG. 6. Selective sorption on acid-leached ferrierite (sample: AJP-60A).

Shortened synthesis times and the use of seed crystals resulted in smaller average crystallite sizes, as judged by microscope observation. Sorption rates and capacities for *n*-heptane on both seeded and unseeded preparations, after a standard HCl treatment, are given in Table 3. Sorption rates were higher for the smaller crystal sizes in the short-term runs, but so were the capacities. Rates which were normalized by dividing by the respective capacities were fairly constant, indicating no difference in the kinetic controlling step for sorption.

To establish the critical pore diameter, sorbates having a range of molecular sizes were tested. In Fig. 6, sorption rates and capacities for 2-methylpentane and toluene are compared to those for *n*-heptane on an acid-leached ferrierite. Only about 10 μl/g of 2-methylpentane or toluene was sorbed, and the rates were slow (even lower sorptions, 3–4 μl/g, were found on the best ferrierite samples). In Fig. 7, the sorption capacities are plotted as a function of the molecular diameters. The latter were estimated using van der Waal's radii of the outer atoms in each molecule; they are 4.9 Å for *n*-paraffins, 5.6 Å for isoparaffins, and 6.7 Å for benzene rings. Actual "effective" diameters may be quite different, but the sharp demarcation found between *n*-paraffins and isoparaffins (4.9–5.6 Å) is in accord with estimates of the main channel openings, 5.2 Å (*4*) and 5.4 Å (*3*). The capacity of 85 μl/g found for water, propane, and *n*-pentane is a maximum value for the main channels (Table 4) and sets

TABLE 3

EFFECT OF SYNTHESIS PREPARATION TIME ON RATE AND CAPACITY OF *n*-HEPTANE SORPTION[a]

Catalyst[b] No.	Preparation time (hr)[c]	Initial rate (mg/min)	Final wt (mg)	Normalized initial rate (min^{-1})	Capacity (ml/g)
AJP-3-2	72 (U)	.78	4.4	0.177	0.035
AJP-3-3	72 (U)	0.96	4.9	0.196	0.039
AJP-3-18	8 (S)	1.65	8.0	0.206	0.068
AJP-3-21	4 (S)	1.47	7.1	0.207	0.058
AJP-3-23	2 (S)	1.17	5.8	0.202	0.050

[a] 200 mg sample charge.
[b] All catalysts were acid leached for 12 hr.
[c] U = unseeded, S = seeded.

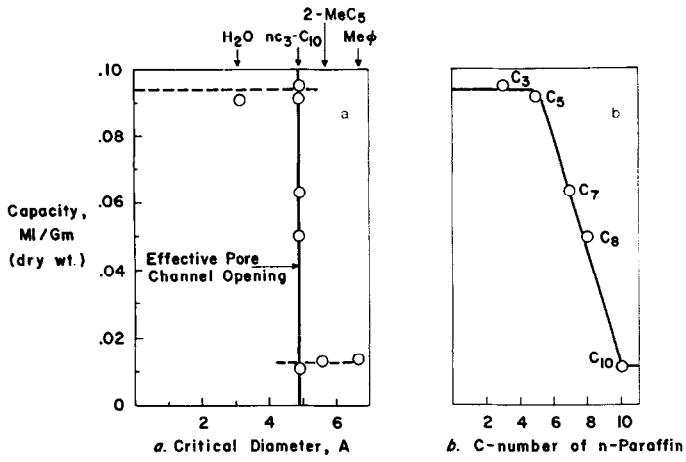

FIG. 7. Sorption capacity as a function of critical molecular diameter (catalyst AJP-60A).

a maximum average diameter of 5.5 Å for them.

Larger *n*-paraffins were not taken up easily (Fig. 7b); for *n*-decane the sorption capacity filled in the allotted time was no greater than that of an isoparaffin. This must be due in part to much slower sorption rates for larger *n*-paraffins. Also, long hydrocarbon chains must be extended rather fully; the densities of sorbed molecules may be much lower than those of normal liquids. However, some of the higher capacity for smaller molecules may be in the cavities accessible by eight-membered ring openings. If this is true, then the main channel diameter and volume are much lower than the maximum values estimated above.

TABLE 4
PHYSICAL DIMENSIONS OF FERRIERITE

Unit cell			
Composition	$(M)_6Al_6Si_{30}O_{72}\cdot 18H_2O$		
Dimensions	19.2 × 14.1 × 7.5 Å [Ref. (*2*)]		
Vol/unit cell	2028 Å^3		
Main channels			
Type, No.	Ten ring, two per unit cell		
Dimensions (2)	4.2 × 5.4 Å [Ref. (*3*)] (5.5 Å)[a]		
Cross section	18 Å^2 (24 Å^2)[a]		
Vol/unit cell	270 Å^3 (360 Å^3)[a]		
M^+	Na^+	H^+	H_3O^+
MW (g/mol)	2618	2486	2594
Vol (cc/g)	0.467	0.491	0.471
Density (g/cc)	2.14	2.04	2.12
Main channel vol (μl/g)	62 (83)[a]	66 (87)[a]	63 (84)[a]

[a] Maximum value derived from measured water loss of Na form.

After sorption of an isoparaffin or an aromatic molecule, the sorption capacity for *n*-paraffins decreased. Table 5 gives data for several ferrierite samples, demonstrating that isoparaffins were particularly effective. When *n*- and isoparaffins were sorbed concurrently, however, the blocking was greatly reduced; the total for toluene and heptane sorbed together was nearly equal to the sum of the separate sorptions. A small *n*-paraffin, hexane, was not blocked as effectively as octane, and as the pores were cleaned out (and perhaps enlarged) by acid treatment and extraction by chelating agents, the blocking effects diminished (Table 5B and C). It was thought that the effect of 2-methylpentane (Table 5A) might be due to the fact that its unbranched end could enter a channel, but that the molecule would then become stuck because its branched end could not enter. However, an isoparaffin branched at both ends was also effective for blocking *n*-paraffin entry.

Fortunately, the presence of *n*-paraffins during sorption is sufficient to keep enough of the pore mouths open so that ferrierite can function as a selective *n*-paraffin sorbent. A hydrogen–ferrierite sorbed 15–20

TABLE 5
SELECTIVE SORPTION ON FERRIERITE

	Compound	Capacity (μl/g)
A. AJP-1-60A, Acid leached 8 hr		
Separate sorption:	2 MP[a]	13
	Toluene	13
	Heptane	63
Consecutive sorption:	2 MP	13
	Heptane	2
	Toluene	13
	Heptane	32
Concurrent sorption:	2 MP Heptane	44
	Toluene Heptane	72

	Capacity (μl/g)			
B. Sorbed separately:	Octane	Hexane	2,5 DMH[a]	Toluene
AJP-1-57[b]	30	28	4	3
AJP-1-57A[c]	40	42	5	3
AJP-1-57Y[d]	40	40	5	4
AJP-1-57X[e]	40	41	8	8
C. Sorbed consecutively:	2,5 DMH; octane	2,5 DMH; hexane		Toluene; hexane
AJP-1-57	4, 5	4, 24		3, 22
AJP-1-57A	5, 11	5, 35		3, 32
AJP-1-57Y	5, 22	5, 37		4, 37
AJP-1-57X	8, 30	8, 36		8, 30

[a] MP = methylpentane, DMH = dimethylhexane.
[b] Acid leached 8 hr in HCl.
[c] Acid leached 16 hr in HCl.
[d] Acid leached 8 hr in HCl, extracted 16 hr with acetylacetone.
[e] Acid leached 16 hr in HCl, extracted 20 hr with EDTA, acid leached another 8 hr.

μl/g indiscriminately from a stream of 1:1:5 by volume heptane:2,4-dimethylpentane:toluene at 20°C, but then completely adsorbed 40 μl/g more of heptane, without adsorbing more of the other two components, before breakthrough of heptane in the product stream. The heptane flow rate, and thus the minimum sorption rate, was 1 μl/g/min in this experiment, with a helium carrier flow of 10 cc/g/min. Desorption at 200°C in helium yielded no toluene or 2,4-dimethylpentane, and only 60% of the sorbed heptane. Also, the catalyst yellowed and cracking products (C_1–C_4 hydrocarbons) were formed; the selective *n*-paraffin capacity decreased rapidly in subsequent sorption–desorption cycles. The cracking activity was neutralized by back exchange with sodium or lithium ions, but at the cost of losing most of the *n*-paraffin sorption capacity. Only about 10 μl/g of *n*-heptane could be selectively sorbed by Na- and Li-ferrierites. A freshly back-exchanged Li-ferrierite sorbed 40 μl/g, but after air calcination at 500°C it became active for cracking again, and after a second Li exchange its capacity dropped to 10 μl/g.

TABLE 6
SELECTIVE SORPTION ON STEAMED FERRIERITE AT 20°C

Sample	AJP-3-18 (seeded run, 12 hr HCl leaching)
Steaming	1 hr at 750°C in 30 cc/g/min H_2O + 30 cc/g/min helium
Selective adsorption	From 7.0 μl/g/min of *n*-heptane, 2,4-dimethylpentane and toluene (1:1:5) in 100 cc/g/min helium at 25°C; desorption, 1 hr at 300°C in 100 cc/g/min helium

Cycle	Sorption at heptane breakthrough (μl/g)	
1	Heptane	49
	Toluene + 2,4 DMP	5
2	Heptane	40
	Toluene + 2,4 DMP	0.5
3	Heptane	42
	Toluene + 2,4 DMP	0.5
4	Heptane	41
	Toluene + 2,4 DMP	0.5
5	Toluene alone	0.1
6	2,4 DMP alone	0.3

Steaming of hydrogen ferrierite at 750°C caused a drastic decrease in its cracking activity (*vide infra*). The structure remained intact and the pore system still took up *n*-paraffins selectively. This simple treatment yielded an excellent sorbent for the removal of *n*-paraffins from a hydrocarbon stream. As shown in Table 6, repetitive sorption–desorption cycles were possible in which 40 μl/g of heptane was removed from a heptane–dimethylpentane–toluene stream. Virtually all of the heptane desorbed at 200–300°C, and no cracking was observed. Under the same conditions (1 μl/g/min heptane at $P/P_0 = 0.05$, 20°C), a Linde 5A sieve also adsorbed about 50 μl/g at breakthrough, although its equilibrium capacity was much higher (150 μl/g vs 60 μl/g for ferrierite).

Catalyst Activity

Hydrogen forms of ferrierite produced by acid treatment of the Na forms were tested for activity and selectivity in the cracking of hydrocarbons. In preliminary experiments, the cracking of *n*-octane and 2,5-dimethylhexane was tested at 300–600°C. The cracking reactions obeyed first-order kinetics. A first-order rate constant was calculated as $k_1 = -\ln(1 - x)/t$, where x is the fractional conversion and t is a superficial contact time defined as the catalyst volume divided by the volumetric flow rate of the feed stream. In Fig. 8, variations in the cracking rate constants are shown for *n*-octane and 2,5-dimethylhexane over one of the initial preparations. It is evident that diffusion limitations are quite important in cracking of paraffins on ferrierite. The apparent activation energies are 7 and 10 kcal/mol for 2,5-dimethylhexane and *n*-octane, respectively. These are in the normal diffusion-controlling region, being much lower than the values of 38 kcal/mol found for thermal cracking (Fig. 8) and 30 kcal/mol over other aluminosilicates (*19*). Product distributions for a freshly calcined catalyst at 300 and 500°C are given in Table 7. The hydrogen content in the products at 300°C was greater than that in the reactants. The initial catalytic activities were very high, like those of other zeolites (*20*), but the catalysts coked rapidly in the absence of

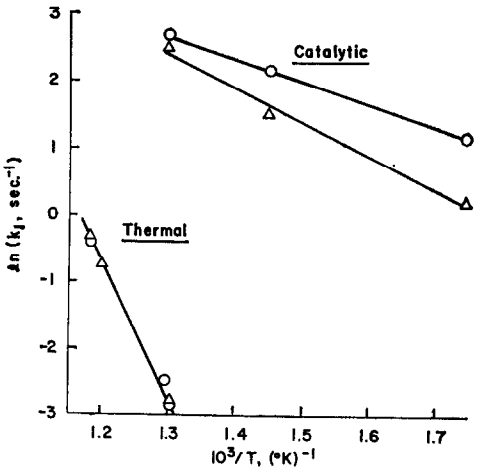

FIG. 8. Paraffin cracking over hydrogen ferrierite-rates vs temperature; (△) *n*-octane, (○) 2,5; dimethylhexane.

TABLE 7
PRODUCT DISTRIBUTIONS IN PARAFFIN CRACKING OVER FERRIERITE[a]

	Product mole fraction			
	n-Octane cracking		2,5-Dimethylhexane cracking	
Product	500°C	300°C	500°C	300°C
Methane	0.040	0	0.127	0.004
Ethane	0.052	0.004	0	0
Propane	0.139	0.143	0.036	0.013
Isobutane	0.041	0.244	0.139	0.442
Butane	0.059	0.109	0.025	0.026
Isopentane	0.005	0.105	0.031	0.148
Pentane	0.021	0.030	0.002	0.002
Total alkanes	0.357	0.635	0.360	0.635
Ethylene	0.197	0.012	0.137	0.010
Propylene	0.297	0.167	0.312	0.169
Butenes	0.149	0.142	0.191	0.169
Pentenes	trace	0.044	trace	0.017
Total alkenes	0.643	0.365	0.640	0.365
H/C ratio (2.250 in octane)	2.240	2.326	2.237	2.322
[iso-(C_4 + C_5)-alkanes]/ [*n*-(C_4 + C_5)-alkanes]	0.6	2.5	6.3	21

[a] Conditions: Ca 1.5 atm He (no hydrogen); 2 μl pulses in 45 cc/min flow over 0.20 g catalyst (AJP-1-2A); (0.1% Na).

hydrogen and eventually the hydrogen content of the products balanced that of the reactants. The selectivity for *n*-paraffin cracking (compared to that for isoparaffins) was not very high on the first preparations of ferrierite, which had starting ratios of 12:1 for SiO_2/Al_2O_3 and were run at 290°C. This may have been due to impurities such as mordenite.

Variation in *n*-octane cracking activity at 400°C with *n*-octane sorption capacity is shown in Fig. 9 for a series of catalysts extracted for different times with HCl. A linear relation was found. However, the activity for 2,5-dimethylhexane cracking also increased in the same direction and the selectivity for *n*-paraffin cracking was nearly constant. Since the sodium content decreased with extraction time, the increases in cracking activity may also have been due to higher catalyst acidities. It is felt that much of the cracking was occurring on the external surfaces of these ferrierite crystals and on impurities.

Attempts to permanently deactivate the external surfaces of hydrogen ferrierite crystals by treatment with KCl, after the pores were filled with a hydrocarbon such

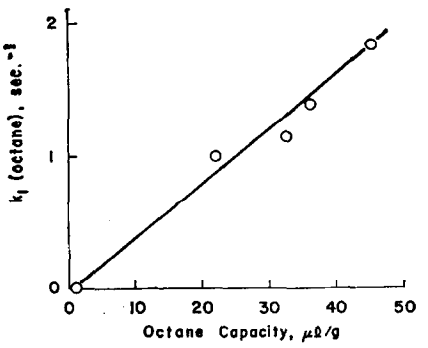

FIG. 9. Variation of cracking rate with adsorption capacity; *n*-octane over HCl-extracted ferrierite, 400°C.

as hexane, were temporarily successful. Initial cracking rates for isoparaffins decreased by factors of five or more while the *n*-paraffin rates were only slightly changed. However, calcination restored the original selectivities as the alkali ions apparently migrated into the crystal interior and protons migrated out to the surface. Attempts to permanently remove external surface acid sites, by removing aluminum from the lattice with complexing agents, also failed. Aluminum was very resistant to removal, and when conditions were made severe enough so that it was removed from ferrierite, silicon was also removed. Large defects were produced, sorption capacity for molecules such as toluene was increased, and the cracking selectivity for *n*-paraffins was not improved.

Since the acid treatment required to activate Na-ferrierites gave catalysts which were not too selective for *n*-paraffin cracking, and a primary objective of the research was to produce a selective catalyst, TMA ions were introduced into the synthesis in order to produce an active catalyst more directly. At the same time, the SiO_2/Al_2O_3 ratio in the starting gels was reduced to 10, corresponding more closely to that of the ferrierite product, and the synthesis temperatures were raised to 300°C and above in order to minimize crystallization of mordenite.

Although calcination of Na-TMA-ferrierites increased their BET areas from 7 to 8 m^2/g to about 100 m^2/g, and developed 10–20 $\mu l/g$ adsorption capacities for hydrocarbons, the sodium content was still too

TABLE 8
CRACKING COMPARISON: ACID-LEACHED FERRIERITE (AJP-1 SERIES) VS AMMONIUM ION-EXCHANGED TMA-FERRIERITE (AJP-2 SERIES)

		AJP-2-5	
	AJP-1-57A[a]	NH-1-60[b]	NH-1-62[b]
		Rate constants (sec^{-1} at 500°C)	
Hexane	3.17	2.30	2.67
Heptane	3.80	2.07	2.23
Octane	5.00	1.73	1.90
2-Methylpentane	1.63	0.11	0.14
2,5-Dimethylhexane	2.67	0.29	0.47
(Hx/2 MP)	(2)	(22)	(19)
(Oct/2,5 DMH)	(2)	(6)	(4)
		Rate constants (sec^{-1} at 400°C)	
Hexane	0.48	0.46	0.57
Heptane	0.83	0.47	0.58
Octane	1.11	0.47	N.M.
2-Methylpentane	0.11	0.004	0.006
2,5-Dimethylhexane	1.07	0.019	N.M.
(Hx/2 MP)	(4)	(115)	(95)
(Oct/2,5 DMH)	(1)	(25)	—
		Activation energies (kcal/mole)	
Hexane	19.5	16.7	16.0
Heptane	15.8	15.3	13.9
Octane	15.5	13.4	—
2-Methylpentane	28.0	34.2	30.8
2,5-Dimethylhexane	9.5	28.1	—

[a] Initial values, acid-leached Na-ferrierite.

[b] Values after poisoning with about 50 $\mu l/g$ of toluene, ammonium-exchanged TMA-Na-ferrierite. NH-1-60 exchanged once, NH-1-62 exchanged twice.

high and they were inactive for cracking. Exchange with ammonium ions gave active cracking catalysts, as shown in Table 8. Initially, these catalysts were only slightly more selective than the first acid-leached Na-ferrierites. However, their selectivity for *n*-paraffin cracking increased as they coked, and dramatically increased after an aromatic molecule such as toluene was passed over the catalyst at 400–500°C, as shown in Table 9. This did not occur with the earlier acid-leached Na-ferrierites. The activation energies for isoparaffin cracking on the deactivated catalysts were about 30 kcal/mol, whereas those for *n*-paraffins were only about 15 kcal/mol. Thus, isoparaffins were effectively excluded from the pore system. Selectivity ratios of 20–100 for *n*-paraffin cracking were found at 400°C.

High *n*-paraffin cracking selectivities were also found for acid-treated Na-ferrierites synthesized above 300°C with 10:1 ratios of SiO_2/Al_2O_3 in the starting gels. They were more active but not quite as selective as TMA-based catalysts; the presence of TMA ions semed to result in better crystallized products and fewer impurities, while acid leaching gave higher sorption capacities. A comparison of two good preparations is shown in Table 10, and Fig. 10. The data are for 520°C, an extreme temperature for hydrocracking catalysts, but it was necessary to run at that temperature in order to measure isoparaffin cracking. Even so, isoparaffin cracking rate constants were only slightly greater than

TABLE 9
THE EFFECT OF TOLUENE ON CRACKING SELECTIVITIES OVER FERRIERITE CATALYSTS

Toluene passed (μl/g)	Selectivity[a]	
	AJP-1-57A	AJP-2-5, NH-1-62[b]
None	2.5	1.4
20	2.5	4.3
40	3.2	7.1
60	3.2	11.6
80	3.2	13.4

[a] Ratio of hexane cracking rate constant to 2-methylpentane cracking rate constant at 520°C.

[b] After several regenerations; selectivities on a fresh sample were about twice as high.

TABLE 10
CRACKING SELECTIVITIES OF HYDROGEN FERRIERITE CATALYSTS

Toluene passed (ml/g)	Selectivities in helium[a]	
	AJP-2-13A[b] from Na-Ferrierite	NH-1-64[c] from Na-TMA-Ferrierite
0.00	5	7
0.02	11	23
0.04	13	35
0.06	15	42
0.08	16	48
k_1(sec^{-1}) for hexane		
No toluene	5.3	3.9
0.08 ml/g Toluene	3.0	3.1

[a] Ratio of hexane to 2-methylpentane cracking rate constants at 520°C.

[b] After HCl treatment.

[c] After calcination at 450°C and NH_4NO_3 exchange.

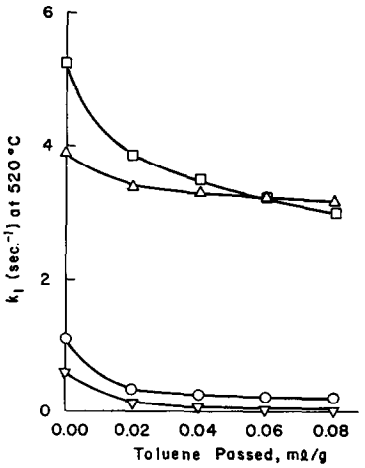

FIG. 10. Cracking activity of hydrogen ferrierite: (□) hexane over HCl-treated Na-ferrierite, (○) 2-methylpentane over HCl-treated ferrierite, (△) hexane over NH_4NO_3-exchanged Na, TMA-ferrierite, (▽) 2-methylpentane over NH_4NO_3-exchanged Na, TMA-ferrierite.

TABLE 11
EFFECTS OF SEEDING ON SORPTION CAPACITY AND CRACKING ACTIVITY

	Sorption capacity (μl/g)		Cracking constant[a] (sec^{-1})	
	2 MP[b]	Hexane	2 MP	Hexane
AJP-2-13A				
72-hr run, unseeded	2.2	60	1.42	1.68
AJP-3-18A				
8-hr run seeded	6.0	63	3.68	5.35
Ratio (seeded/unseeded)	2.7	1.0	2.6	3.2

[a] Initial activities at 500°C.
[b] 2 MP = 2-methylpentane.

thermal rate constants after toluene deactivation.

It was noted that smaller average crystallite sizes were formed in short-term, seeded syntheses. One of these was compared directly to a long-term, unseeded run which gave a comparable *n*-hexane sorption capacity. As shown in Table 11, the sorption capacity for 2-methylpentane and the cracking rate constants for both 2-methylpentane and hexane were three times greater for the catalyst derived from the seeded run. This is inversely proportional to the relative crystallite sizes as estimated crudely by microscope observations. A larger external surface area (for 2-methylpentane adsorption and cracking) is expected for smaller crystals, and more channel openings to reduce diffusional limitations in hexane cracking. However, the internal pore volume (for hexane sorption) should remain constant, as observed.

Hydrogen ferrierite calcined to 500°C is too active for cracking to be used as an *n*-paraffin sorbent for more than a few sorption–desorption cycles, but when fully exchanged with alkali ions, to eliminate cracking, the channels are blocked so that very little sorption capacity is left. It was found that the cracking activity could also be nearly eliminated by steaming at 750°C. This left the structure intact (by X-ray analysis) and only slightly lowered the sorption capacity, but it reduced the cracking activity by a factor of 100 as shown in Table 12.

CONCLUSIONS

1. Synthetic Na-ferrierite forms as the major phase from a gel with starting composition $Na_2O:Al_2O_3:10\ SiO_2$ (200 H_2O), at 300–325°C and 1250–1750 psi. Its unit cell composition is then $Na_6Al_6Si_{30}O_{72}\cdot 18H_2O$. The synthesis time may be reduced from 72 hr to 2 hr by seeding.

2. A mixed Na, TMA-ferrierite forms under the same conditions when tetra-

TABLE 12
DEACTIVATION OF CRACKING ACTIVITY

Catalyst AJP-3-18A	Sorption capacity (μl/g)		Cracking constant[a] (sec^{-1})	
	2 MP[b]	Hexane	2 MP	Hexane
Fresh	6.0	63	0.40	1.80
Steamed[c]	5.5	55	0.003	0.018
Ratio (fresh/steamed)	1.1	1.1	130	100

[a] At 400°C.
[b] 2 MP = 2-Methylpentane.
[c] For 1 hr at 750°C.

methylammonium hydroxide is added; up to 2 TMA ions/unit cell may be incorporated.

3. Treatment of Na-ferrierite with mineral acids or ammonium ion exchange of calcined Na, TMA-ferrierites produces hydrogen ferrierites with high *n*-paraffin sorption capacities and cracking activities.

4. The sorption capacities of isoparaffins and aromatics are low in hydrogen ferrierite, and the cracking rates for these compounds may be reduced to low levels by pretreating hydrogen ferrierite at 400–500°C with toluene.

5. The cracking activity of hydrogen ferrierite may be greatly reduced by steaming at 750°C, but this treatment does not significantly change the sorption selectivities or capacities for *n*-paraffins; the structure remains intact.

Acknowledgments

We thank Dr. John Freel for the electron microscope work, Dr. E. R. Tucci for acid treatments of ferrierite samples, and W. Faust, H. Haraznak, J. Tolley, and T. Worek for technical assistance. Thanks are also due to the Gulf Research & Development Company for support of this work and for permission to publish it.

References

1. Graham, R. P. D., *Proc. Trans. Roy. Soc. Can., 3rd Ses., Sect. 4,* 185 (1918).
2. Staples, L. W., *Amer. Mineral.* **40,** 1095 (1955).
3. Vaughn, P. A., *Acta Crystallogr.* **21,** 983 (1966).
4. Kerr, I. S., *Nature (London)* **210,** 294 (1966).
5. Kirov, G. N., and Filizova, L., *God. Sofii. Univ., Geol-George Fak* **59,** 237 (1965); *Chem. Abstr.* **68,** 4836.
6. Alietti, A., Passaglia, E., and Scaini, G., *Amer. Mineral.* **52,** 1562 (1967).
7. Baric, L., *Bull. Sci. Conseil Acad. RSF Yougoslavie* **10,** 177 (1965); *Chem. Abstr.* **65,** 16690.
8. Yajima, S., Nakamura, T., and Ishii, E., *Mineral J.* **6,** 343 1971; *Chem. Abstr.* **77,** 64548.
9. Wise, W. S., Nokleberg, W. J., and Kokinos, M., *Amer. Mineral.* **54,** 887 (1969).
10. Sands, L. B., Proc. Conf. Econ. Geol. Massachusetts, 1966.
11. Coombs, D. S., Ellis, A. J., Fyfe, W. S., and Taylor, A. M., *Geochim. Cosmochim. Acta* **17,** 53 (1959).
12. Senderov, E. E., *Geokhimiya* **9,** 820 (1959).
13. Sands, L. B., *Int. Conf. Molecular Sieves 1st,* p. 71 (1967).
14. Barrer, R. M., and Marshall, D. J., *J. Chem. Soc.* **1964,** 485 (1964).
15. Barrer, R. M., and Marshall, D. J., *Amer. Mineral.* **50,** 484 (1965).
16. Hawkins, D. B., *Mater. Res. Bull.* **2,** 951 (1967).
17. Massoth, F. E., *Chem. Technol.* **1972,** 285 (1972).
18. Bogdanova, V. I., and Belitskii, I. A., *Geol. Geofiz.* **1968,** 44 (1968).
19. Barrer, R. M., and Lee, J. A., *J. Colloid Interface Sci.* **30,** 111 (1969).
20. Miale, J. N., Chen, N. Y., and Weisz, P. B., *J. Catal.* **6,** 278 (1966).